PCCP

PAPER

View Article Online
View Journal | View Issue

Cite this: *Phys. Chem. Chem. Phys.*, 2016, **18**, 28893

Ultrafast excited states dynamics of $[Ru(bpy)_3]^{2+}$ dissolved in ionic liquids†

Mario Borgwardt,[a] Martin Wilke,[a] Igor Yu. Kiyan[a] and Emad F. Aziz*[abc]

Received 15th August 2016,
Accepted 19th September 2016

DOI: 10.1039/c6cp05655e

www.rsc.org/pccp

Room-temperature ionic liquids (ILs) represent a well-known class of materials exhibiting extremely low vapor pressures and high electrochemical stability. These properties make ILs attractive for various applications requiring UHV conditions. Here, we apply 1-ethyl-3-methylimidazolium trifluoromethanesulfonate [EMIM][TfO] as a solvent to investigate the excited state dynamics of the transition metal complex $[Ru(bpy)_3]^{2+}$ with the use of ultrafast XUV photoelectron spectroscopy. This study is aimed to reveal the effect of the IL environment when the frontier molecular orbitals and the states dynamics of the solute need to be addressed. By initiating the electron dynamics with a pump laser pulse of 480 nm wavelength, we can unambiguously characterize the kinetics of the excited states of $[Ru(bpy)_3]^{2+}$ and determine their absolute binding energies. From a global fit analysis of the transient signal, the binding energies of the initially populated metal-to-ligand charge-transfer state ^{1}MLCT and the thermally relaxed ^{3}MLCT are inferred to be −0.2 eV and 0.3 eV, respectively. A three-state model, including the intersystem crossing (ISC) from the ^{1}MLCT to the ^{3}MLCT state and the intramolecular vibrational relaxation (IVR) within the triplet configuration, is used to describe the involved decay processes. The kinetic constants of (37 ± 10) fs for the ISC and (120 ± 20) fs for the IVR are found to be in agreement with the values previously reported for aqueous solution. The obtained results open up exciting new possibilities in the field of liquid phase spectroscopy.

1 Introduction

Room-temperature ionic liquids (ILs) have been extensively investigated as promising new materials for numerous applications.[1–3] The attractiveness of this class of materials stems from their manifold interesting physicochemical properties[4–7] such as the liquid state over a wide range of temperatures, chemical inertness, high ionic conductivity, and very low vapor pressures.[8,9] The latter makes ILs perfectly suitable for applications under UHV conditions, required for many surface-sensitive techniques. Among those, photoelectron spectroscopy (PES) represents one of the most powerful methods to study interfaces and has been proven to provide unique data for the near-surface composition, chemical state identification, and the valence band structure.[10–15] Most of the PES investigations were primarily focused on the IL samples themselves, whereas the use of ILs as solvents opens up a range of exciting new experimental possibilities to study isolated molecules and complexes in solutions with the use of the PES technique.[16–20]

In the present work, the excited states dynamics of the ruthenium transition metal complex $[Ru(bpy)_3]^{2+}$ dissolved in 1-ethyl-3-methylimidazolium trifluoromethanesulfonate [EMIM][TfO] are examined. The excited state properties of this complex were already studied using other spectroscopic methods.[21–26] Therefore, it was chosen as a model system for studying the effect of the IL environment on the intramolecular electron transfer reactions in this class of compounds. Here, femtosecond time-resolved PES in the spectral XUV range is applied and the capabilities of this method in both revealing the intramolecular relaxation kinetics and determining the binding energies of the involved states are demonstrated. For this purpose, the laser-based technique of high-order harmonic generation[27,28] (HHG) is applied to provide the necessary photon energy of up to 40 eV and to achieve a high temporal resolution, enabling us to probe the ground state as well as the excited states simultaneously on an ultrafast timescale. To the best of our knowledge, there are no studies reported regarding the application of ILs as solvents in PES experiments to investigate the energetic and dynamic properties of solutes. The present work can therefore be seen as a first benchmark to explore the advantages of this approach in the field of liquid-phase

[a] *Joint Laboratory for Ultrafast Dynamics in Solutions and at Interfaces (JULiq), Institute of Methods for Material Development, Helmholtz-Zentrum Berlin, Albert-Einstein-Strasse 15, D-12489 Berlin, Germany. E-mail: emad.aziz@helmholtz-berlin.de; Tel: +49 30 8062 15003*
[b] *Department of Physics, Freie Universität Berlin, Arnimallee 14, 14195 Berlin, Germany*
[c] *Institute for Molecular Science, Myodaiji, Okazaki 444-8585, Japan*

† Electronic supplementary information (ESI) available: Detailed description of the cross-correlation on the bare ionic liquid, an analysis of the long-term stability and sample damage, time traces as well as energy traces at specific time delays and binding energies. See DOI: 10.1039/c6cp05655e

spectroscopies and to answer important scientific questions about the IL–solute interaction.

This study is organized as follows. At first, the steady state XUV emission of the bare IL is characterized, including the PES spectrum of the valence shell as well as its stability under continuous XUV illumination. Subsequently, the photoemission yield of $[Ru(bpy)_3]^{2+}$ dissolved in [EMIM][TfO] is analyzed and the spectral contributions from the valence-band molecular orbitals of the metal compound are examined. The central part of this study is to follow the excited states dynamics of the metal complex initiated by applying a pump laser beam of 480 nm wavelength. The findings are compared to the previously reported description of the photo-cycle, and the correlation between the solute and its IL environment is discussed.

2 Experimental section

2.1 Sample preparation

The liquid sample was prepared by mixing $[Ru(bpy)_3]Cl_2$ (Sigma-Aldrich, 37.4 mg, 0.05 mmol) with [EMIM][TfO] (IoliTec, 0.5 ml), yielding a solute's concentration of 100 mM which is close to the solubility limit. The mixture was shaken for several hours resulting in a dark solution without visible residual precipitates. A loop formed of a copper wire was dipped into the solution so that a droplet of less than 1 μl content was attached to it. The loop was mounted inside the UHV experimental chamber and electrically connected to the electron spectrometer. A typical residual gas pressure in the chamber was in the range of 10^{-7} mbar during the experiment. The samples were prepared immediately prior to measurements. Because of the *ex situ* sample preparation, special attention was paid to possible surface contamination. To exclude any influence by contaminants, measurements on the bare IL were conducted (see ESI,† S1: cross-correlation on the bare IL: temporal resolution). Slight changes in the XUV emission spectrum of the sample were observed when the IL was exposed to the XUV beam on a time scale of several hours. Detailed analysis of the long-term stability of the sample can be found in the ESI,† S2 (S2: long term stability and sample damage).

2.2 Time-resolved photoemission spectrometer

A detailed description and characterization of the XUV light source can be found elsewhere.[29,30] Briefly, a Ti:sapphire laser system delivering 2.5 mJ, 800 nm, 25 fs pulses at a repetition rate of 5 kHz was used to generate the visible pump and the XUV probe beams. The laser output is split and approximately 1.5 mJ pulse energy is applied for the frequency up-conversion *via* the HHG process. The 21st harmonic of the fundamental frequency, with a photon energy of 32 eV, is selected with the use of a reflective off-center zone plate and refocused by a toroidal mirror into the experimental chamber. The XUV photon flux in the interaction region was $\sim 10^6$ photons per pulse, as measured by means of a calibrated photodiode. Another part of the laser output was used for pumping of an optical parametric amplifier (OPA) to generate pulses at 480 nm wavelength, corresponding to a photon energy of 2.58 eV. The spot sizes of the pump and the probe beams at the sample were 500 μm and 100 μm, respectively. The pump pulse energy was 1 μJ, corresponding to a photon flux of 1.3×10^{15} photons per cm^2 in the interaction region. A computer-controlled delay stage was used in the pump beam path to vary the time delay between the pump and probe pulses. A time response of (110 ± 5) fs (FWHM) in the present experiment was inferred from a cross-correlation measurement carried out on the bare ionic liquid sample.

The kinetic energy spectra of photoelectrons were measured with the use of a time-of-flight (TOF) electron spectrometer THEMIS 600 delivered by SPECS. The spectrometer is equipped with a cylindrical multi-element electrostatic lens that maps electrons emitted from the sample onto a detector positioned at the end of the drift region. The lens can be operated in different modes, differing in the electron acceptance angle, the spectral energy range, and the energy resolution. In the drift mode (DM), the electrostatic lenses are disabled and the spectrometer performs as a classical drift tube with an acceptance angle of ±1°, determined by the ratio of the detector aperture and the spectrometer length. This mode was used to acquire steady-state photoelectron spectra in a wide kinetic energy range. The wide-angle mode (WAM) yields the highest acceptance angle of ±15°, though the kinetic energy scale is limited to a certain range around a predefined kinetic energy. This mode was used for the acquisition of spectra with a high signal-to-noise ratio in an energy range sufficient to reveal the spectral components of XUV ionization from the ground state of the ruthenium complex and from the transient states. The spectral energy resolution was mainly determined by the HHG bandwidth convoluted with the spectrometer resolution. An energy resolution of 0.1 eV was derived from a calibration measurement by recording the XUV ionization spectrum of argon gas. The absolute binding energies of the probed electronic states were inferred from the measured kinetic energies of photoelectrons. The binding energies will be given with respect to the Fermi level defined from the energy calibration routine.

3 Results and discussion

3.1 Steady state PES study of bare ILs

The energy structure of the valence band of [EMIM][TfO] is inferred from the steady-state XUV spectrum shown in Fig. 1, recorded without application of the pump beam. The spectrum exhibits a number of pronounced peaks that were fitted to Gaussian profiles (see dashed lines). Using the previously reported results of DFT calculations,[11,15] one can assign some of those features. The three peaks at 10.0, 11.5, and 14.9 eV binding energies can be clearly attributed to the fluorine 2p orbitals of the TfO^- anion. The peak with the highest amplitude, lying at 10.0 eV, was chosen as a reference to calibrate the binding energy scale according to the corresponding literature value from ref. 12 and 15. Direct determination of the absolute binding energy scale, *e.g.* by referencing to the Fermi level of gold, was complicated because of the space charge

effect induced in ILs. This effect originates from the accumulation of positive charges at the IL surface due to the reduced electric conductivity of the sample.[31,32] The energy calibration in the previous studies was commonly accomplished by referencing the spectra, including the peak at 10.0 eV, to the aliphatic carbon 1s state with a binding energy of 285.0 eV relative to the Fermi level.[14] Since the reference core states are not accessible by means of XUV photons applied in this study, the above mentioned peak of TfO^- was chosen here as the reference. The peaks in the range of binding energies between 4 and 9 eV cannot be unambiguously assigned neither to the anion nor cation states.[33] However, the ionization potential of the solvent, given by the minimum amount of energy required to remove an electron from the solvent molecules, represents an important characteristic. A large ionization potential is preferable, so that an overlap with the solute's HOMO is avoided, leading to a better resolution of the solute spectral contributions and a higher signal-to-noise ratio. Fig. 1b shows the magnified spectral range of the highest occupied orbitals of [EMIM][TfO]. The onset of the occupied states is determined by the crossing point of the horizontal line representing the noise level with the straight inclined line describing the slope of the HOMO energy peak in the [EMIM][TfO] spectrum. (Note the logarithmic vertical scale in Fig. 1b.) By means of this procedure, an energy onset value of 2.6 eV was found. This value needs to be considered when analyzing the HOMO level position of the ruthenium complex, as discussed in the following section.

3.2 Steady state PES study of $[Ru(bpy)_3]^{2+}$ dissolved in ILs

The steady state spectrum of the $[Ru(bpy)_3]^{2+}$ complex dissolved in [EMIM][TfO] was recorded under the same experimental conditions as those used in the study of the bare solvent. A comparison between both measurements is presented in Fig. 2. For a better visibility of the solute contributions, the difference between the two steady state spectra is shown on the right-hand side.

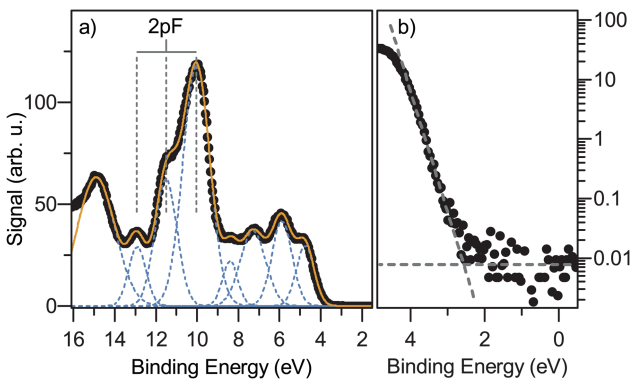

Fig. 1 Steady state XUV spectrum of the bare [EMIM][TfO]. Panel (a) shows the entire recorded spectral range. The contributions of individual energy peaks are represented by Gaussian profiles (dashed lines) obtained from the fit. The pronounced contributions of the fluorine 2p orbitals of the TfO^- anion are indicated by vertical dashed lines. In panel (b) the spectral range encompassing the highest occupied orbitals is shown in greater detail on a logarithmic scale.

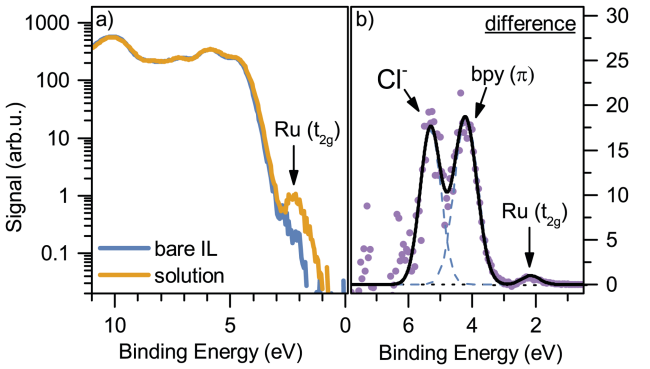

Fig. 2 (a) Steady-state XUV spectra of photoelectrons recorded for the bare IL (blue line) and for the 100 mM solution of $[Ru(bpy)_3]^{2+}$ (yellow line), plotted on a logarithmic scale. The emission peak from the $[Ru(bpy)_3]^{2+}$ ground state arises at 2.3 eV binding energy. (b) The difference between the two spectra shown in panel (a), revealing the emission spectrum of the solute. Contributions from the Cl^- counter ion and from the t_{2g} and π orbitals of the metal complex are indicated.

The contribution of the HOMO band of the dye to the spectrum is apparent at a binding energy of 2.3 eV, and can be assigned to the ruthenium t_{2g} molecular orbital. Thus, it is clearly separated from the IL contribution exhibiting the 2.6 eV energy onset. Such a spectral composition is highly preferable for time-resolved PES studies since it results in a high quality of the transient signal, not suffering from an additional and potentially strong background from solvent ionization. For the $[Ru(bpy)_3]^{2+}$ complex dissolved in water, a binding energy value of 6.81 eV of the $Ru(t_{2g})$ orbital can be found in the literature.[34] However, this number refers to the vacuum level as it is a common procedure to define the absolute energy scale in water jet experiments. Taking the spectrometer's work function of 4.4 eV into account,[30] the binding energy obtained in this work is in good agreement with the literature value.

Adjacent to the dye HOMO band, a second, even stronger double-peak contribution is apparent in the solute spectrum at higher binding energies (Fig. 2b). This spectral region is attributed to ionization from the Cl^- 3p ground state of the counter ion and from the ligand-donated π orbitals of $[Ru(bpy)_3]^{2+}$.[34] The signal was fitted in this range to a sum of two Gaussian profiles with maxima arising at binding energies of 4.2 eV and 5.3 eV, respectively. A binding energy of 9.6 eV relative to the vacuum level was previously reported for aqueous Cl^- 3p.[34,35] Taking the spectrometer's work function into account, the peak at 5.3 eV can be, thus, clearly assigned to the ionization of Cl^-. The assignment of the peak at 4.2 eV to ionization from the ligand-donated π orbitals of the metal complex is consistent with the previous study, where this emission band was shown to lie between the $Ru(t_{2g})$ and the Cl^- energy peaks.[34] For a related ruthenium polypyridyl complex, DFT calculations revealed a relative band offset of 2 eV between the metal-center-localized t_{2g} orbital and the ligand-donated π orbitals.[36] This value is close to the present result, demonstrating the energy difference of 1.9 eV.

The ionization yield of $[Ru(bpy)_3]^{2+}$ represents an important issue, since it influences considerably the acquisition time

required to obtain sufficient statistic of the transient signal. One should emphasize that the experiment was conducted with a $[Ru(bpy)_3]^{2+}$ concentration close to the solubility limit. However, the solute contribution appears to be rather weak in the emission spectra. Without knowledge of the ionization cross sections of the solvent and the solute, it is difficult to draw any solid conclusion with regard to the absolute signal amplitude and the actual concentration of the solute at the surface. Further efforts are needed to clarify the surface composition compared to the bulk properties, and to develop approaches enabling us to possibly enrich the concentration of the metal complex at the surface.

3.3 Transient signal

Fig. 3 illustrates the photochemical cycle of $[Ru(bpy)_3]^{2+}$. Optical excitation leads to a charge transfer transition from the metal-center-localized d orbital of the singlet ground state ($^1A_1$) to the ligand-donated orbital of the excited metal-to-ligand charge-transfer (^{1}MLCT) state. The prepared excited singlet state undergoes ultrafast intersystem crossing, leading to the formation of the long-lived triplet ^{3}MLCT state, with nearly unity quantum yield. It is commonly accepted that this process occurs on a time scale well below 100 fs,[37,38] whereas much shorter transition times of 15 fs[39] have also been reported. From luminescence measurements in liquid solutions, the radiative decay of ^{3}MLCT was found to exhibit a time constant on the order of 1 μs with an overall quantum yield of 5%[40,41] in H_2O and 9%[41] in CH_3CN. The reason for the rather low quantum yield is the competing non-radiative decay channel to the triplet metal-centered states (^{3}MC) *via* an efficient internal conversion (IC) mechanism. For $[Ru(bpy)_3]^{2+}$, the ^{3}MC state was found to be energetically higher than the ^{3}MLCT state.[40,42,43] Therefore, the quenching of the ^{3}MLCT luminescence *via* the ^{3}MC state appears to be thermally activated.[44,45] However, the population of this intermediate state remains negligible at all times due to the much higher relaxation rate of ^{3}MC to $^1A_1$. Another simultaneously occurring energy disposal mechanism is the internal vibrational relaxation (IVR) within the complex. For the initially populated high vibrational levels of the ^{3}MLCT state, femtosecond fluorescence spectroscopy revealed their decay *via* IVR being completed within 300 fs.[39,46] This value has been the subject of intense discussions, since larger values of up to picoseconds have also been reported.[37] At room temperature, the luminescence does not exhibit any structure and originates from the thermally equilibrated excited states. The luminescence band maximum lies at approximately 2 eV photon energy.[40]

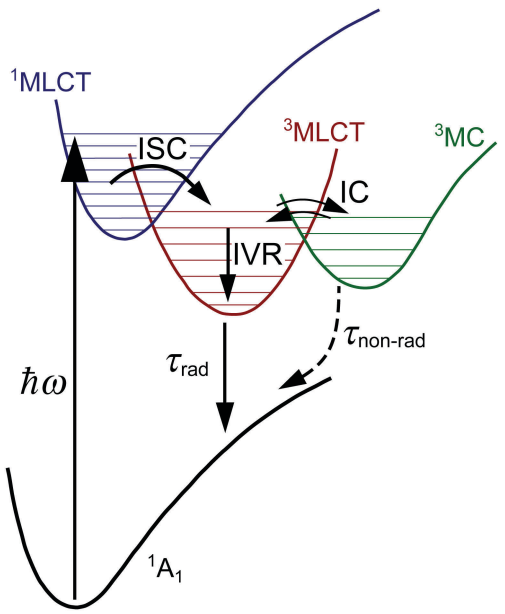

Fig. 3 The photochemical cycle of $[Ru(bpy)_3]^{2+}$ depicted in a simplified energy level diagram. Absorption of visible light promotes the Ru 4d electron from the ground $^1A_1$ state to the excited ^{1}MLCT state, where it undergoes ultrafast intersystem crossing into the ^{3}MLCT state. The ^{3}MLCT state decays *via* two channels: non-radiatively *via* internal conversion to the ^{3}MC state and radiatively to the ground state with a time decay constant of up to 1 μs. IVR represents a simultaneously occurring energy disposal mechanism.

The transient PES study was performed with a pump beam of 480 nm wavelength, giving rise to the resonant excitation of the ^{1}MLCT state. The electron population distribution among the transient states is probed by applying the 21st harmonic of 32 eV photon energy. The transient signal (TS) was derived by subtracting the XUV spectra recorded at negative delay times as a background from the pump–probe spectra. The color map given in Fig. 4a presents the two-dimensional dependence of the TS on the binding energy and the time delay.

The TS exhibits several distinct features which are first discussed qualitatively below. A detailed analysis of the data by using a global fit and the derivation of kinetic values and binding energies of the involved states are presented in the next section. In the vicinity of zero time delay (±100 fs), the TS exhibits a strong contribution at energies between 2 and 3.5 eV. This feature can be unambiguously attributed to the cross-correlation (CC) signal originating from the bare IL substrate. Its temporal width is found to be 110 fs (FWHM), which reproduces the value from pump–probe measurements on the bare IL sample (see ESI,† S1) and depicts the time response of the spectrometer throughout this work. The CC component represents an unavoidable contribution to the TS. However, due to its favorable sidewise appearance in the TS at higher binding energies, a clear spectral separation of the sample-related TS signal is achieved. This represents another important issue which one needs to consider when choosing an IL as a solvent for a transient PES experiment. In addition to the requirement of large IL's ionization potential in order to avoid the overlap between the solvent and solute XUV spectra, the IL spectrum shifted by one photon energy of the pump beam should not coincide with the ionization signal from a transient state of the solute.

The negative value of the TS at binding energies in the vicinity of 2.3 eV, corresponding to the Ru t_{2g} molecular orbital, arises due to the depletion of the ground state of $[Ru(bpy)_3]^{2+}$ caused by photo-excitation. The ground state depletion is formed within the pump pulse duration and remains constant over the pump–probe time interval shown in Fig. 4. Even on a larger timescale of up to 2 ns (not shown here), no changes in

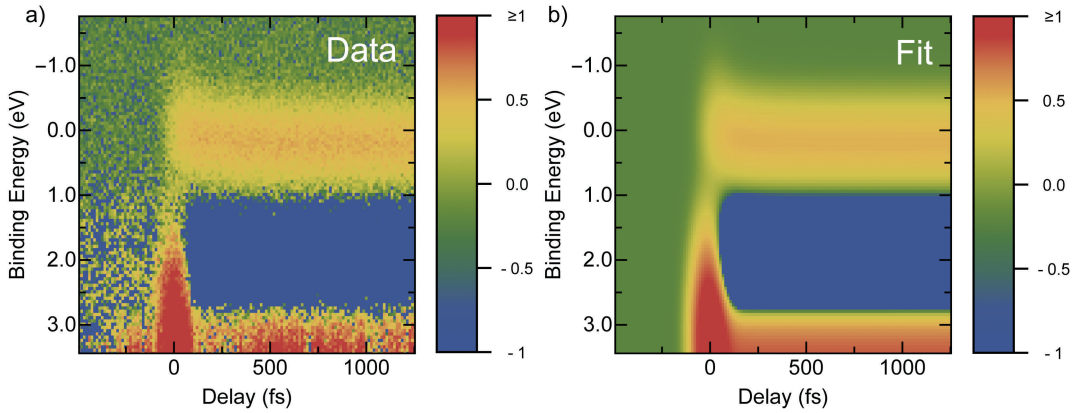

Fig. 4 2D color maps of the background-subtracted transient signal obtained for a 100 mM solution of $[Ru(bpy)_3]^{2+}$ in [EMIM][TfO]. Panel (a) shows the experimental data. The reproduction of experimental results by a global fit with the use of the sequential model (see the text) is presented in panel (b).

the negative TS signal could be observed. This characterizes the long lifetime of molecular excitation, associated with a weak relaxation to the ground-state configuration. Another long-lived feature appears as a positive signal at binding energies larger than 3 eV. Presumably, it is due to emission from a ligand-donated π orbital of an excited metastable triplet state of the Ru complex. Since this feature lies in the vicinity of the ground state depletion, it needs to be considered in the global fit analysis presented below.

In the range of binding energies below 1 eV, the TS exhibits a more complex behavior. This spectral region encompasses the excited states of $[Ru(bpy)_3]^{2+}$ including the initially populated ^{1}MLCT as well as the states involved in the subsequent relaxation dynamics. The signal onset is clearly shifted on the time scale with respect to the CC peak determining zero time delay. It indicates that this part of the TS originates from resonantly populated states with lifetimes on the order or larger than the CC duration. Particularly noteworthy is the spectral drift of the component which is centered at approximately −0.2 eV at early time delays and is shifted to 0.3 eV at time delays larger than 500 fs. From this spectral drift one can conclude that following the initial excitation of the ^{1}MLCT state, the early relaxation dynamics involves a sequential population of a number of states possessing different binding energies. The spectral decomposition of the TS is discussed in detail in Section 3.4. Similar to the ground state depletion, this shifted spectral component remains constant over the range of long time delays applied in the experiment and, apparently, can be assigned to the long-lived ^{3}MLCT. Another proof of this assignment is given by the difference in binding energy of 2.0 eV between the ^{3}MLCT and the ground state, which fits well to the wavelength of fluorescence originating from the thermally equilibrated ^{3}MLCT excited state. It is important to note that this occurrence is not self-evident since the PES and fluorescence spectroscopic methods obey different selection rules. The fluorescence signal is defined by the overlap integral between the occupied vibrational ^{3}MLCT states and the ground state, which is not the case for PES. However, since the thermal equilibrium is reached, only a minor discrepancy is expected.

3.4 Kinetic model

The TS shown in Fig. 4 was analyzed in terms of a global fit. The kinetic model implemented on the basis of previously described relaxation channels has the form:

$$^1\mathrm{A}_1 \xrightarrow{P(t)} {}^1\mathrm{MLCT} \xrightarrow{k_1} {}^3\mathrm{MLCT_{hot}} \xrightarrow{k_2} {}^3\mathrm{MLCT_{cold}} \xrightarrow{k_3} {}^1\mathrm{A}_1/{}^3\mathrm{MC} \quad (1)$$

where $P(t)$ denotes the photo-excitation rate of the ^{1}MLCT state from the ground state ^{1}A$_1$. The rate constants k_{1-3} characterize the subsequent transitions to the hot and then cold ^{3}MLCT state and the decay of ^{3}MLCT$_{cold}$. As discussed above, this decay occurs either through the direct recombination to the ground state or *via* the population transfer to the ^{3}MC state. Both dissipation channels are much slower than the transitions between the MLCT states and, therefore, a more detailed consideration of the ^{3}MLCT$_{cold}$ decay mechanism is not essential for the description of ultrafast electron dynamics in the picosecond range considered in Fig. 4. Moreover, the same nanosecond time constant was found for both the ^{3}MLCT decay and the ground state recovery.[44] This suggests that the constant k_3 introduced above describes the relaxation rate from ^{3}MLCT$_{cold}$ to the ground state. In the kinetic model, the triplet state is divided into two components (^{3}MLCT$_{hot}$ and ^{3}MLCT$_{cold}$) to account for the vibrational cooling within this state. This can be seen as a simplified approach to take into account a finite number of vibrational states with their specific binding energies and relaxation rates.

The following system of differential equations describes the above depicted population dynamics:

$$\begin{aligned}
\frac{\mathrm{d}[^1\mathrm{MLCT}]}{\mathrm{d}t} &= P(t)[^1\mathrm{A}_1] - k_1[^1\mathrm{MLCT}] \\
\frac{\mathrm{d}[^3\mathrm{MLCT_{hot}}]}{\mathrm{d}t} &= k_1[^1\mathrm{MLCT}] - k_2[^3\mathrm{MLCT_{hot}}] \\
\frac{\mathrm{d}[^3\mathrm{MLCT_{cold}}]}{\mathrm{d}t} &= k_2[^3\mathrm{MLCT_{hot}}] - k_3[^3\mathrm{MLCT_{cold}}] \\
\frac{\mathrm{d}[^1\mathrm{A}_1]}{\mathrm{d}t} &= -P(t)[^1\mathrm{A}_1] + k_3[^3\mathrm{MLCT_{cold}}]
\end{aligned} \quad (2)$$

The system of rate equations was solved numerically with the initial condition that all the involved excited states are unpopulated and only the ground state $^1A_1$ is initially occupied. The ionization signal from the individual states was calculated by convoluting their transient population with the temporal envelope of the XUV probe pulse. Hereby the probe step was assumed to be non-saturated and the emission energy peaks were considered to have Gaussian envelopes. For both pump and probe pulses, Gaussian time envelopes were considered with a constraint that their convolution yields the measured CC of 110 fs width. Apart from the ionization yield from the four states considered in the kinetic model, the CC signal as well as the signal above 3 eV binding energy, denoted by Q_0, were taken into account in the numerical routine. The transition rates k_{1-3} and the emission spectra of transient states were obtained from a global fit of the kinetic model results to the measured TS. The fit yielded very good reproduction of the experimental data, as can be seen from Fig. 4. The obtained values of fit parameters, such as the binding energies E_b, the bandwidths ΔE_b, and the decay time constants τ_d of the transient states, are summarized in Table 1. The lifetime of (37 ± 10) fs (inverse of the transition rate k_1) of the ^{1}MLCT state is shorter than the time response of 110 fs in the present experiment. One should note that the measurement of time constants considerably smaller than the laser pulse duration is possible if the precise time zero is known.[47] In the present study, the time zero is inferred from the global fit by taking simultaneously into account the CC yield, which appears sidewise in the TS at higher binding energies as discussed above. The error bars of the time constants and binding energies reported in Table 1 were derived by the global fit routine on the basis of the statistical scatter of data points obtained from 65 individual delay scans. Additionally, time traces as well as energy traces at specific time delays and binding energies, respectively, are shown in Fig. S4 and S5 in the ESI,† including the TS decomposition to individual contributions from the involved states obtained from the fit.

The initially populated ^{1}MLCT state is found to lie at a binding energy of (-0.2 ± 0.2) eV. The energy difference to the $^1A_1$ ground state is therefore given by 2.5 eV and matches within the error estimate of the applied excitation photon energy of 2.58 eV. This finding supports the assignment of this spectral component to the singlet ^{1}MLCT state. Its lifetime given in Table 1 is very similar to the intersystem crossing time constant that was reported by Bhasikuttan *et al.*[37] However, the much shorter decay time on the order of 15 fs reported in ref. 39 cannot be confirmed. One should note that the cross-correlation width imposes limitations on the time resolution in the present experiment, so that any rigorous conclusion on such a short timescale appears to be difficult.

The vibrational relaxation from the $^3MLCT_{hot}$ to the $^3MLCT_{cold}$ was found to take place within 120 fs. Yoon *et al.* obtained from time-resolved Raman spectroscopy a time constant of 110 fs,[38] which agrees well with our findings. Other literature values mostly refer to the complete disappearance of the signal from vibrationally hot states, and provide time constants within 300 fs.[39,46] The number provided in the present work represents the inverse value of the fitted transition rate k_2, meaning that the amplitude of the hot state decreased by a factor of $1/e$. Considering a signal decrease by one order of magnitude, one can recalculate a relaxation time of 280 fs, which is in good agreement with the reported values. The present work reveals that a total energy dissipation of approximately 0.6 eV occurs within this time interval. Since in previous experiments a higher photon energy of 3.1 eV was applied, even higher dissipation values of 1.1 eV were found.[39,46] Such a fast dissipation raised the discussion to what extent the solvent environment influences the intramolecular excited states dynamics. Cannizzo *et al.*[39] argued that due to the fast progression of the energy dissipation, a transfer to the solvent is unlikely and rather an energy transfer from high-frequency modes to low-frequency modes takes place, as reported for the case of bacteriorhodopsin.[48] In contrast, Damrauer *et al.*[46] claimed that the intramolecular vibrational relaxation is connected to solvent reorganization due to the formation of an excited state exhibiting a large dipole moment. The similarities between the reported values for commonly used solvents (H_2O in ref. 39 and CH_3CN in ref. 45) and the present value obtained for the IL environment indicate that solute–solvent interactions are only of minor importance. However, theoretical modeling of the electrostatic interactions in ILs remains poor until today,[49] preventing any valuable prediction of the correlation strength between the solvent and the solute.

One should note that the found energy positions of the two excited states (^{1}MLCT, $^3MLCT_{hot}$) exhibit uncertainties because of their broad and overlapping character as well as because of the limited experimental temporal and spectral resolution. Additional complication arises if one would consider that the intersystem crossing and the intramolecular vibrational relaxation take place simultaneously, making the modeling much more complex. However, the position of the long-lived $^3MLCT_{cold}$ can be unambiguously determined from the TS at time delays beyond 500 fs. In the description of the early-time dynamics, an attempt was made to prove the validity of the three-state model by omitting the intermediate $^3MLCT_{hot}$ state. As a result the fastest decay constant was found to be larger than 100 fs and, therefore, the fit did not reproduce the spectral components at the binding energies below -0.2 eV which evolve on a much faster timescale. Since the ultrafast component could not be adequately reproduced, the three-state model described above was found to yield a better quantitative agreement. On the other hand, introducing even more states in addition to the $^3MLCT_{hot}$ certainly would lead to more flexibility and better fit results on the basis of the residual analysis. However, due to the above

Table 1 Lifetime constants (τ_d), binding energies (E_b), and bandwidth (ΔE_b) of the ^{1}MLCT, $^3MLCT_{cold}$ and $^3MLCT_{hot}$ states obtained from the global fit analysis of the transient signal with the use of eqn (1)

State	E_b (eV)	ΔE_b (eV)	τ_d
^{1}MLCT	-0.2 ± 0.2	1.2	(37 ± 10) fs
$^3MLCT_{hot}$	0.1 ± 0.2	0.9	(120 ± 20) fs
$^3MLCT_{cold}$	0.3 ± 0.1	0.9	>1 ns
$^1A_1$	2.3 ± 0.1	1.2	—

mentioned limitations, a more complex kinetic model with a larger number of fit parameters would not yield a better understanding of the relaxation mechanisms.

4 Conclusion

The excited states dynamics of $[Ru(bpy)_3]^{2+}$ dissolved in ILs was investigated by means of time resolved photoelectron spectroscopy. Hereby, the general applicability of ILs as solvents was characterized in detail. The analysis of the bare ILs showed a favorable ionization potential, enabling us to clearly separate the HOMO state contributions of the solute from the solvent's features in the XUV photoemission spectrum. This makes ILs beneficial if the valence band structure and dynamics of different samples need to be addressed. Steady state XUV spectra revealed the HOMO band of the $[Ru(bpy)_3]^{2+}$ molecule with the absolute binding energy being very similar to those found in aqueous solution. The transient signal of $[Ru(bpy)_3]^{2+}$ was analyzed by applying a global fit procedure. The kinetic model included the intersystem crossing from the ^{1}MLCT to the ^{3}MLCT state as well as the intramolecular vibrational relaxation within the triplet state. The obtained transition rates were found to be in good agreement with literature values and provided evidence that the solvation dynamics has only a minor influence on the ultrafast deactivation processes. The initially populated ^{1}MLCT state and the thermally relaxed ^{3}MLCT state could be clearly separated, whereas for the intermediate species the description relies on the kinetic model used in the fit analysis.

Summarizing, this study demonstrates the potential of using ILs as solvents. The particular problem arising from sample evaporation, which needs to be overcome in PES experiments, can be solved due to the extremely low vapor pressure of ILs. The ultrafast photoemission spectroscopy applied here has proven to be a powerful tool for exploring both the ultrafast electron dynamics and the absolute binding energies of the involved states. As a next step, more complex mechanisms such as the electron transfer reaction between different species could be investigated, which represents a wide field of potential applications in photochemistry and photobiology.

Acknowledgements

This work is funded by the European Research Council, Grant No. 279344 (E. F. A.), and by the Helmholtz-Gemeinschaft *via* the VH-NG-635 Grant (E. F. A.).

References

1 P. Wasserscheid and W. Keim, *Angew. Chem., Int. Ed.*, 2000, **39**, 3772–3789.
2 R. D. Rogers and G. A. Voth, *Acc. Chem. Res.*, 2007, **40**, 1077–1078.
3 H. Weingärtner, *Angew. Chem., Int. Ed.*, 2008, **47**, 654–670.
4 T. Welton, *Chem. Rev.*, 1999, **99**, 2071–2084.
5 F. van Rantwijk and R. A. Sheldon, *Chem. Rev.*, 2007, **107**, 2757–2785.
6 N. V. Plechkova and K. R. Seddon, *Chem. Soc. Rev.*, 2008, **37**, 123–150.
7 P. Hapiot and C. Lagrost, *Chem. Rev.*, 2008, **108**, 2238–2264.
8 O. Aschenbrenner, S. Supasitmongkol, M. Taylor and P. Styring, *Green Chem.*, 2009, **11**, 1217–1221.
9 M. Bier and S. Dietrich, *Mol. Phys.*, 2010, **108**, 211–214.
10 D. Yoshimura, T. Yokoyama, T. Nishi, H. Ishii, R. Ozawa, H. Hamaguchi and K. Seki, *J. Electron Spectrosc. Relat. Phenom.*, 2005, **144–147**, 319–322.
11 O. Höfft, S. Bahr, M. Himmerlich, S. Krischok, J. A. Schaefer and V. Kempter, *Langmuir*, 2006, **22**, 7120–7123.
12 K. Kanai, T. Nishi, T. Iwahashi, Y. Ouchi, K. Seki, Y. Harada and S. Shin, *J. Chem. Phys.*, 2008, **129**, 224507.
13 K. R. J. Lovelock, I. J. Villar-Garcia, F. Maier, H.-P. Steinrück and P. Licence, *Chem. Rev.*, 2010, **110**, 5158–5190.
14 I. J. Villar-Garcia, E. F. Smith, A. W. Taylor, F. Qiu, K. R. J. Lovelock, R. G. Jones and P. Licence, *Phys. Chem. Chem. Phys.*, 2011, **13**, 2797–2808.
15 A. Ulbrich, M. Reinmöller, W. J. Beenken and S. Krischok, *J. Mol. Liq.*, 2014, **192**, 77–86.
16 E. F. Smith, I. J. V. Garcia, D. Briggs and P. Licence, *Chem. Commun.*, 2005, 5633.
17 F. Maier, J. M. Gottfried, J. Rossa, D. Gerhard, P. S. Schulz, W. Schwieger, P. Wasserscheid and H.-P. Steinrück, *Angew. Chem., Int. Ed.*, 2006, **45**, 7778–7780.
18 J.-P. Mikkola, P. Virtanen, H. Karhu, T. Salmi and D. Y. Murzin, *Green Chem.*, 2006, **8**, 197–205.
19 M. Ruta, G. Laurenczy, P. J. Dyson and L. Kiwi-Minsker, *J. Phys. Chem. C*, 2008, **112**, 17814–17819.
20 R. Tao, S. Miao, Z. Liu, Y. Xie, B. Han, G. An and K. Ding, *Green Chem.*, 2009, **11**, 96–101.
21 J. P. Paris and W. W. Brandt, *J. Am. Chem. Soc.*, 1959, **81**, 5001–5002.
22 A. Vlček, *Coord. Chem. Rev.*, 2000, **200–202**, 933–978.
23 J. Ferguson, F. Herren, E. Krausz, M. Maeder and J. Vrbancich, *Coord. Chem. Rev.*, 1985, **64**, 21–39.
24 A. Juris, V. Balzani, F. Barigelletti, S. Campagna, P. Belser and A. von Zelewsky, *Coord. Chem. Rev.*, 1988, **84**, 85–277.
25 V. Balzani, A. Juris, M. Venturi, S. Campagna and S. Serroni, *Chem. Rev.*, 1996, **96**, 759–834.
26 W. Gawelda, M. Johnson, F. M. F. de Groot, R. Abela, C. Bressler and M. Chergui, *J. Am. Chem. Soc.*, 2006, **128**, 5001–5009.
27 X. F. Li, A. L'Huillier, M. Ferray, L. A. Lompré and G. Mainfray, *Phys. Rev. A: At., Mol., Opt. Phys.*, 1989, **39**, 5751–5761.
28 T. Brabec and F. Krausz, *Rev. Mod. Phys.*, 2000, **72**, 545–591.
29 J. Metje, M. Borgwardt, A. Moguilevski, A. Kothe, N. Engel, M. Wilke, R. Al-Obaidi, D. Tolksdorf, A. Firsov, M. Brzhezinskaya, A. Erko, I. Y. Kiyan and E. F. Aziz, *Opt. Express*, 2014, **22**, 10747.
30 M. Borgwardt, M. Wilke, T. Kampen, S. Mähl, W. Xiang, L. Spiccia, K. M. Lange, I. Y. Kiyan and E. F. Aziz, *J. Phys. Chem. C*, 2015, **119**, 9099–9107.
31 L.-P. Oloff, M. Oura, K. Rossnagel, A. Chainani, M. Matsunami, R. Eguchi, T. Kiss, Y. Nakatani, T. Yamaguchi, J. Miyawaki,

M. Taguchi, K. Yamagami, T. Togashi, T. Katayama, K. Ogawa, M. Yabashi and T. Ishikawa, *New J. Phys.*, 2014, **16**, 123045.
32 R. Al-Obaidi, M. Wilke, M. Borgwardt, J. Metje, A. Moguilevski, N. Engel, D. Tolksdorf, A. Raheem, T. Kampen, S. Mähl, I. Y. Kiyan and E. F. Aziz, *New J. Phys.*, 2015, **17**, 093016.
33 M. Reinmöller, A. Ulbrich, T. Ikari, J. Preiß, O. Höfft, F. Endres, S. Krischok and W. J. D. Beenken, *Phys. Chem. Chem. Phys.*, 2011, **13**, 19526.
34 R. Seidel, M. Faubel, B. Winter and J. Blumberger, *J. Am. Chem. Soc.*, 2009, **131**, 16127–16137.
35 B. Winter and M. Faubel, *Chem. Rev.*, 2006, **106**, 1176–1211.
36 J. E. Monat, J. H. Rodriguez and J. K. McCusker, *J. Phys. Chem. A*, 2002, **106**, 7399–7406.
37 A. C. Bhasikuttan, M. Suzuki, S. Nakashima and T. Okada, *J. Am. Chem. Soc.*, 2002, **124**, 8398–8405.
38 S. Yoon, P. Kukura, C. M. Stuart and R. A. Mathies, *Mol. Phys.*, 2006, **104**, 1275–1282.
39 A. Cannizzo, F. van Mourik, W. Gawelda, G. Zgrablic, C. Bressler and M. Chergui, *Angew. Chem., Int. Ed.*, 2006, **45**, 3174–3176.
40 J. V. Houten and R. J. Watts, *J. Am. Chem. Soc.*, 1976, **98**, 4853–4858.
41 K. Suzuki, A. Kobayashi, S. Kaneko, K. Takehira, T. Yoshihara, H. Ishida, Y. Shiina, S. Oishi and S. Tobita, *Phys. Chem. Chem. Phys.*, 2009, **11**, 9850.
42 J. P. Sauvage, J. P. Collin, J. C. Chambron, S. Guillerez, C. Coudret, V. Balzani, F. Barigelletti, L. D. Cola and L. Flamigni, *Chem. Rev.*, 1994, **94**, 993–1019.
43 A. Islam, N. Ikeda, A. Yoshimura and T. Ohno, *Inorg. Chem.*, 1998, **37**, 3093–3098.
44 Q. Sun, S. Mosquera-Vazquez, L. M. L. Daku, L. Guénée, H. A. Goodwin, E. Vauthey and A. Hauser, *J. Am. Chem. Soc.*, 2013, **135**, 13660–13663.
45 Q. Sun, B. Dereka, E. Vauthey, L. M. Lawson Daku and A. Hauser, *Chem. Sci.*, 2016, DOI: 10.1039/c6sc01220e.
46 N. H. Damrauer, G. Cerullo, A. Yeh, T. R. Boussie, C. V. Shank and J. K. McCusker, *Science*, 1997, **275**, 54–57.
47 T. Hertel, E. Knoesel, M. Wolf and G. Ertl, *Phys. Rev. Lett.*, 1996, **76**, 535–538.
48 T. Kobayashi, T. Saito and H. Ohtani, *Nature*, 2001, **414**, 531–534.
49 M. N. Kobrak and H. Li, *Phys. Chem. Chem. Phys.*, 2010, **12**, 1922.

